

An investigation of the influence of the size distribution of seeding particles on LDA velocity data in the vicinity of a large velocity gradient

P. J. Thomas^{a)} and K.-A. Bütetisch

Deutsche Forschungsanstalt für Luft- und Raumfahrt, Institut für Experimentelle Strömungsmechanik, Bunsenstrasse 10, D-37073 Göttingen, Germany

(Received 16 September 1992; accepted 9 July 1993)

The influence of the properties of the size distribution of seeding particles on the results of laser Doppler anemometry (LDA) velocity measurements in the vicinity of a large velocity gradient downstream of an aerodynamic shock is studied numerically. Accounting for the differing velocity lag of particles of different sizes the average velocity and the pertaining rms values are determined in the relaxation region within which the particles adjust towards the changed flow velocity downstream of the shock. It is shown how the average velocity and the rms value depend on the mean particle size and the density of the particle material. It is demonstrated in a numerical simulation how the LDA system's "amplitude limit," which can offer a means of excluding the contribution of large particles towards the experimental results, affects the average velocity and the rms value to be measured in the relaxation region. Experimental LDA data of velocity measurements across an oblique shock are presented. A good qualitative agreement of the numerical and the experimental results is found.

I. INTRODUCTION

Any fluid flow velocity measurement involving a particle tracer technique such as laser Doppler anemometry (LDA) relies on the information obtained from seeding particles suspended in and transported with the fluid. Hence, one key assumption of such techniques must be that the seeding particles fed into the flow follow changes of the flow velocity with a negligible velocity lag. While this assumption can usually be regarded as being satisfied for small to moderate velocity changes, this is, however, not necessarily the case for a large velocity gradient like that occurring across an aerodynamic shock.

A velocity determination by means of LDA at a measuring location in a flow field usually consists of as many as several hundred separate, independent, single velocity measurements carried out on individual seeding particles crossing the LDA's measuring volume. The results of these single measurements are then averaged to yield an average velocity and its pertaining rms value. There are numerous publications on LDA dealing with either some aspects of theoretically investigating the motion of single particles (e.g., Maxwell and Seasholtz,¹ Walsh,² Nichols,³ Tedeschi *et al.*,⁴ Maurice⁵), or experimentally measuring the flow velocity across shocks (e.g., Krishnan *et al.*,⁶ d'Humieres *et al.*⁷). Nevertheless, none of the available theoretically based publications have taken into account that the particles' sizes of commonly used seeding materials are distributed corresponding to a more or less broad size distribution. Particles of different sizes reveal a different velocity lag in the relaxation region within which they adjust to a changed flow velocity. The different velocity lag will lead to a contribution towards the total measured rms value at

measuring locations within the relaxation region. This contribution which is solely due to the size distribution of the seeding particles is often mistakenly interpreted as turbulence of the flow. It is therefore of great importance to know how far experimentally obtained LDA data are biased by the particles' response behavior towards a large velocity gradient. Authors of experimental publications involved with laser Doppler anemometry who are well aware of this problem very often conclude that it is therefore strongly advisable to use a monodisperse particle size distribution. While such a distribution would certainly overcome the problem it is, however, not readily accessible for everyday experimental practice. Those seeding particles (i.e., latex particles) that can in principle be produced with a very narrow almost monodisperse size distribution can, due to technical limitations, often only be produced in number densities too low for the desired specific application. This leads to low data rates and long measuring times. The study of the literature has shown that the seeding particles commonly used in practice are, in general, far from being monodisperse.

The purpose of this paper is to investigate numerically the contribution due to the particle size distribution towards the rms value in the region downstream of an aerodynamic shock and to compare these results qualitatively to experimental LDA velocity data. It is understood that this contribution depends on the flow conditions, the exact properties of the size distribution, as well as on the type of seeding particles used. The results presented here are therefore to be regarded as a first guideline for the experimenter to develop a feeling for the importance and the order of magnitude of this contribution towards the total rms value in similar experimental applications.

II. PARTICLE MOTION

Consider a small (order of size: μm), nondeformable, spherical particle not disturbing the flow. Neglecting wall

^{a)}Present address: Department of Applied Mathematics and Theoretical Physics, University of Cambridge, Silver Street, Cambridge, CB3 9EW, England.

effects, the motion of this particle in a fluid can be described by the Basset–Bousinesq–Oseen (BBO) equation which is given in the notation of Soo⁸ by

$$\begin{aligned} \frac{4\pi}{3} r_p^3 \rho_p \frac{d\mathbf{U}_p}{dt_p} &= \frac{4\pi}{3} r_p^3 \rho_p G(\mathbf{U}_F - \mathbf{U}_p) - \frac{4\pi}{3} r_p^3 \frac{\partial P}{\partial \mathbf{r}} \\ &+ \frac{1}{2} \frac{4\pi}{3} r_p^3 \rho_F \frac{d}{dt_p} (\mathbf{U}_F - \mathbf{U}_p) \\ &+ 6r_p^2 \sqrt{\pi \rho_F \mu_F} \\ &\times \int_{t_{p0}}^{t_p} \frac{(d/d\tau)(\mathbf{U}_F - \mathbf{U}_p)}{\sqrt{t_p - \tau}} d\tau + \mathbf{F}_a \end{aligned} \quad (1)$$

with

$$G = \frac{3}{8} C_D \frac{\rho_F}{\rho_p} \frac{1}{r_p} |\mathbf{U}_F - \mathbf{U}_p|, \quad [s^{-1}], \quad (2)$$

where \mathbf{U}_p and \mathbf{U}_F denote particle and fluid velocity, respectively, and ρ_p , ρ_F are the densities of the particle material and the fluid. The radius of the particle is r_p , the viscosity of the fluid is denoted by μ_F and the empirical drag coefficient of the particle is given by C_D . The physical significance of the five terms on the right-hand side of Eq. (1) are as follows. The first term represents the force acting on the particle due to a stationary viscous flow for a particle motion with a relative velocity $|\mathbf{U}_F - \mathbf{U}_p|$. By defining a Reynolds number, Re , as

$$Re = \frac{2r_p |\mathbf{U}_p - \mathbf{U}_F| \rho_F}{\mu_F}$$

and using Stokes' expression for the drag coefficient $C_D = 24/Re$, this term can be seen to be the well-known Stokes law for the force acting on the particle. The second term on the right-hand side of Eq. (1) is due to the pressure gradient in the surrounding fluid. The third term is referred to as added or apparent mass and represents the force required to accelerate the mass of the fluid surrounding the particle and moving with it, the increment being one-half the mass of the fluid displaced ($1/2m_F$). The fourth term on the right-hand side is the so-called Basset integral or Basset history integral. This term accounts for the deviation of the flow from the steady state. The last term on the right-hand side of Eq. (1) denotes external forces such as gravity.

The pressure term disappears in the region of constant flow velocity downstream of the shock. As discussed by Thomas⁹ the influence of the added mass term on the particle motion may be neglected for the experiments carried out. Hughes and Gilliland¹⁰ have shown that the force described by the Basset integral in the case of a flow accelerated at high rates can be many times larger than the viscous drag in the stationary case. The force described by the Basset integral and its influence on the particle motion across the shock investigated is studied in detail by Thomas.^{9,11} It is shown there that this force may be neglected in the case examined here. Furthermore, the influence of external forces will be excluded.

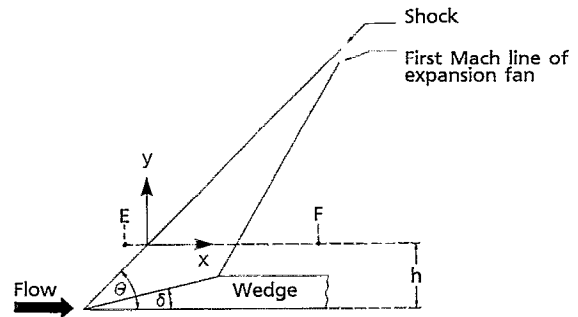


FIG. 1. Wedge, oblique shock, and measuring traverse \overline{EF} .

The simplified equation for the particle motion across the shock, on which the theoretical results of Sec. III are based, is thus

$$\frac{d\mathbf{U}_p}{dt_p} = G(\mathbf{U}_F - \mathbf{U}_p) \quad (3)$$

with G given by Eq. (2). In the general case with the drag coefficient C_D appearing in Eq. (2) written as $C_D(Re, \dots)$, the component form of Eq. (3) consists of two coupled ordinary differential equations for the two components of the flow velocity and has to be solved numerically. If Stokes' expression $C_D = 24/Re$ for the drag coefficient is used, the two equations for the velocity components uncouple and can be solved in closed form. The equation for the drag coefficient C_D used here for the calculations presented is due to Henderson.¹² This equation satisfies a large number of experimental and theoretical results, accounting for compressibility, as well as rarefaction effects, and appears to be among the most accurate of the C_D equations to date. As this equation constitutes a rather lengthy expression it is not stated here expressly. Equation (3) is integrated numerically by the use of the Bulirsch–Stoer method using Turbo Pascal routines suggested by Press *et al.*¹³

With reference to various earlier LDA velocity measurements across oblique aerodynamic shocks generated at wedges of different wedge angles δ (see for instance Krishnan *et al.*,⁶ d'Humieres *et al.*⁷), where the flow velocity was measured at locations along a traverse from a point E to a point F at a height h above the leading edge of the wedge, as indicated in Fig. 1, the theoretical results presented here are given, with respect to the coordinate system x, y used in these publications. Due to the deflection of the flow any particle detected upon crossing the LDA's measuring volume at a measuring location along the traverse \overline{EF} (Fig. 1) has crossed the shock front at a position lying underneath the intersection of \overline{EF} and the shock front. Thus the coordinate system of the particle motion and the measuring system of the LDA (shown in Fig. 1) are not identical. A transformation of the particle motion into the measuring system can be obtained by simple geometrical considerations (see Thomas⁹).

The calculations presented below are based on the particle size distribution of Fig. 2. This size distribution was obtained by means of a TSI APS 33B Aerodynamic Parti-

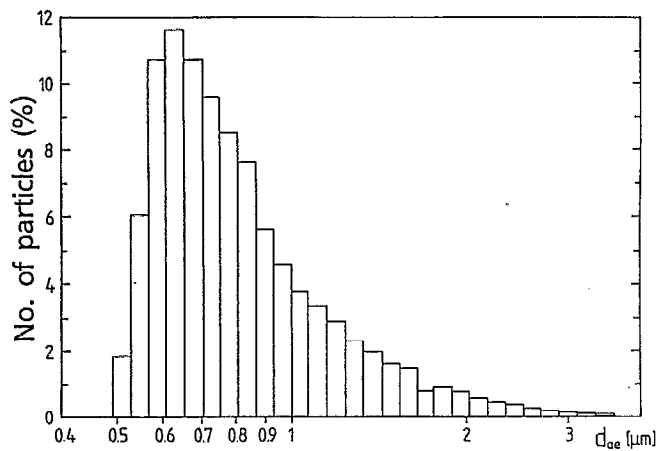


FIG. 2. Measured particle size distribution of the olive oil seeding particles generated by the Laskin nozzle type particle generator.

cle Sizer for olive oil seeding particles generated by a Laskin nozzle type particle generator (see for instance Echols and Young¹⁴). These olive oil seeding particles have been widely used with great success in various types of flows at the DLR, Göttingen, in past years. The average particle diameter of these particles was found to be approximately $0.9 \mu\text{m}$ with a standard deviation of around $0.63 \mu\text{m}$. This size distribution is believed to represent roughly the size distributions of the types of liquid seeding particles most commonly used in experimental applications similar to the one considered here.

For the calculations the particle motion was determined for i different size classes, as they were obtained from the particle sizer, and then transformed into the measuring system of the LDA. The results for both velocity components of a particle size class at any given location along the measuring traverse \overline{EF} were weighted in accordance with the number of particles in that class to obtain an average velocity curve and the respective rms value for each of the two velocity components.

III. RESULTS

All numerical and experimental results presented in this section refer to the component of the flow velocity in the main flow direction (compare Fig. 1). The rms value is given in percent, with respect to the constant free-stream velocity upstream of the shock.

A. Numerical results

The following values for the flow parameters upstream of the shock were assumed throughout the calculations: total pressure, 97 400 Pa; static pressure, 13 650 Pa; total temperature, 291.4 K. Furthermore, a shock angle of $\Theta=47.4^\circ$ to the horizontal, main flow direction was assumed. With the above values the upstream Mach number is $\text{Ma}=1.94$ and the flow velocity in the main flow direction is obtained as 501.5 m/sec upstream and as 386.0 m/sec downstream of the shock. It is moreover assumed

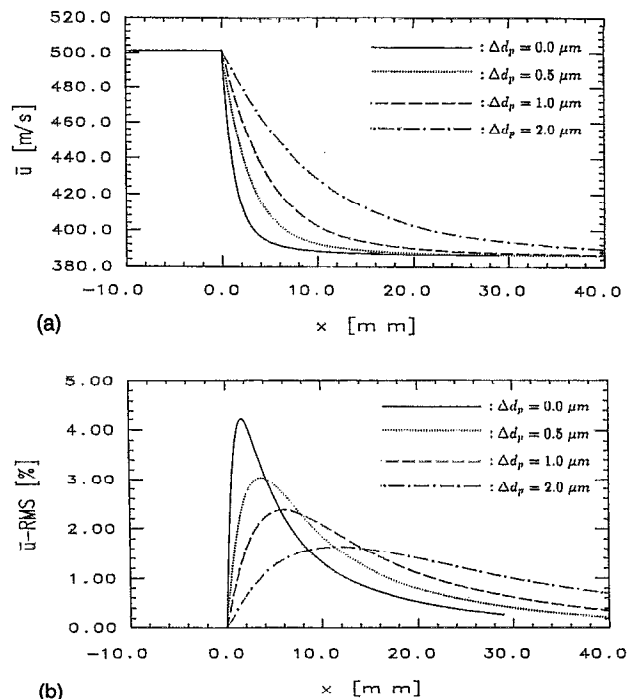


FIG. 3. Expected average velocity and pertaining rms value downstream of the shock for the flow component in the main flow direction as a function of the coordinate x of the LDA's measuring system for particle distributions with different values of the parameter Δd_p ($\rho_p=0.874 \cdot 10^3 \text{ kg/m}^3$).

that just upstream of the shock the velocity of all particles is equal to the upstream flow velocity, hence, the rms value vanishes there.

Figure 3 shows the numerical results, based on the particle size distribution of Fig. 2, obtained for the average velocity and the pertaining rms value downstream of the shock. The different pairs of curves shown correspond to different values of a parameter Δd_p whose meaning is as follows. The results for $\Delta d_p=0.0 \mu\text{m}$ correspond directly to the size distribution of Fig. 2. The results for any value $\Delta d_p \neq 0.0 \mu\text{m}$ correspond to a size distribution that is obtained if the diameter d_{p_i} of each size class i of Fig. 2 is replaced by $d_{p_i} + \Delta d_p$, i.e., if the whole size distribution is shifted towards bigger particle sizes but with the initial shape of the size distribution kept constant. This procedure was chosen to study the contribution towards the rms value for similar distributions which are centered around different mean values.

Figure 3(a) shows how an increase of Δd_p affects the curve obtained for the average velocity. It can be seen that for the original size distribution of Fig. 2, i.e., the curve obtained for $\Delta d_p=0.0 \mu\text{m}$, the particles should adjust to the changed flow velocity to an accuracy of less than 2 m/sec within a distance of approximately 10 mm downstream of the shock position. For increasing Δd_p , this distance grows and can be seen to take on a value of just over 40 mm for the $\Delta d_p=2.0 \mu\text{m}$ case, corresponding to an average particle diameter of around $2.9 \mu\text{m}$. The pertaining curves for the rms value are shown in Fig. 3(b). For the $\Delta d_p=0.0 \mu\text{m}$ case a maximum of around 4% for the rms

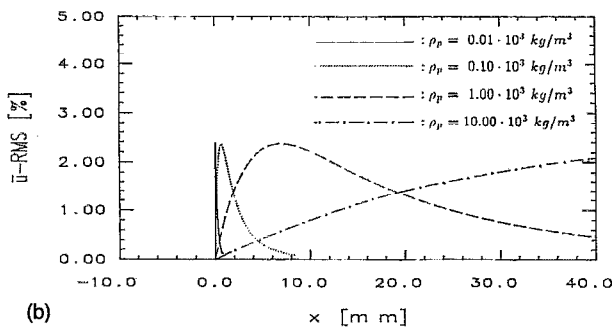
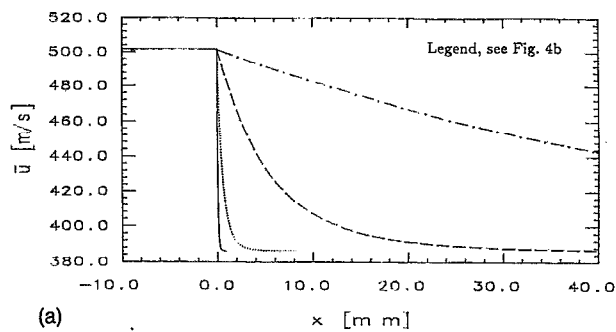


FIG. 4. Expected average velocity and pertaining rms value downstream of the shock for the flow component in the main flow direction as a function of the coordinate x of the LDA's measuring system for a particle distribution with $\Delta d_p = 1.0 \mu\text{m}$ and varying particle density ρ_p .

value is to be expected approximately 1.5 mm downstream of the shock. It can be seen from Fig. 3(b) that for increasing Δd_p the shape of the rms curve broadens and the position of the curve's maximum moves farther downstream of the shock while the rms value itself at the position of the maximum simultaneously decreases.

The influence of the particle density ρ_p on the average velocity and the rms value is shown in Fig. 4 for the particle size distribution with $\Delta d_p = 1.0 \mu\text{m}$. The numerical results are shown here for the value $\Delta d_p = 1.0 \mu\text{m}$ as we will later refer to this figure again. Figure 4(b) shows that for increasing particle density the shape of the rms curve also broadens while the position of the curve's maximum again moves farther downstream of the shock. The rms value itself on the other hand at the position of the maximum stays constant for different values of ρ_p .

In Fig. 5 it is shown how the average velocity and the rms value downstream of the shock are affected if the influence of the larger particles of the size distribution on the numerical result is neglected. This was done to simulate the effect of the use of the data acquisition system's "amplitude limit" on experimental data. If it may be assumed that detected LDA signals with a large signal amplitude correspond to large particles, then the effect of the amplitude limit is to exclude detected signals exceeding some set threshold and, hence, large particles from data evaluation.

Figure 5 shows the numerically obtained results for the size distribution with $\Delta d_p = 0.0 \mu\text{m}$ which are to be expected in an experiment if all those large particles are neglected whose frequency of occurrence is less than 2%, 5%, and 10%, given as a percentage of all particles in the

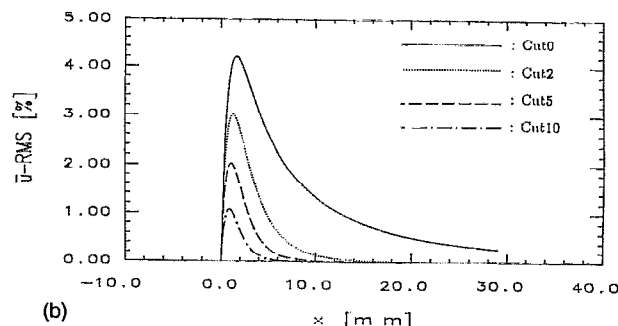
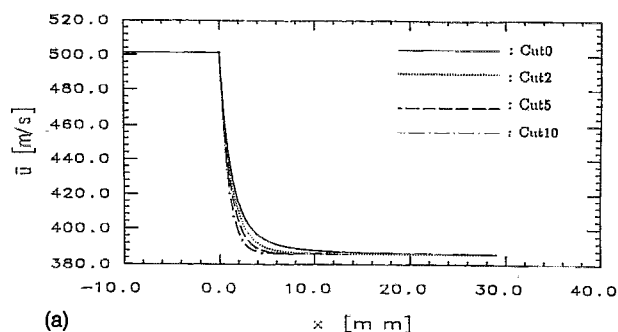


FIG. 5. Numerical simulation of the influence of the amplitude limit on the results of the LDA velocity measurements downstream of the shock. Expected average velocity and pertaining rms value for the flow component in the main flow direction as a function of the coordinate x of the LDA's measuring system for a particle distribution with $\Delta d_p = 0.0 \mu\text{m}$ ($\rho_p = 0.874 \cdot 10^3 \text{ kg/m}^3$).

size distribution. The numerical results obtained with these modified distributions are referred to as Cut 2, Cut 5, and Cut 10, respectively. The curves referred to as Cut 0 are the results obtained when the contribution of all particles is taken into account. It can be seen from the graphs shown in Fig. 5(a) how neglecting increasingly more and more of the "original" distribution's large particles affects the average velocity curve. While the velocity curve for the Cut 0 case approaches the value of the downstream velocity to within the accuracy of less than approximately 2 m/sec at $x \approx 10 \text{ mm}$, this is achieved at $x \approx 4 \text{ mm}$ for the Cut 10 case which corresponds to neglecting a total of approximately 60% of all the particles making up the size distribution. The influence of neglecting the larger particles on the rms value is depicted in Fig. 5(b). The maximum rms value of around 4% for the Cut 0 case reduces to approximately 1% for the Cut 10 case on neglecting more and more of the larger particles, while the width of the graph gets narrower and the position of the maximum is simultaneously moving in the direction of the position of the shock.

B. Experiments, experimental data and comparison with numerical results

We will now present some experimental LDA velocity data obtained for the flow across an oblique aerodynamic shock and compare these data qualitatively to the results of the above numerical simulations.

The shock was generated in the test section of a wind tunnel at the edge of a wedge employing the flow configu-

ration of Fig. 1 and the flow velocity was measured at locations along a traverse EF as indicated. The numerical values of the flow parameters during the collection of all of the experimental data presented in this section were very close to those assumed for the numerical simulations above.

The data were collected using the three-component LDA of the DLR, Göttingen. A detailed description of this LDA can be found in Bütetfisch and Sauerland¹⁵ and in Bütetfisch.¹⁶

The flow configuration considered is two dimensional and thus two components of the LDA are sufficient to determine the relevant velocity components of the flow, namely the velocity component in the main flow direction and the component perpendicular to it due to the deflection of the flow across the shock. (The experimental data displayed in Fig. 7 were collected with the LDA's position relative to the main flow being such that only two LDA components were actively involved in measuring these two flow velocities directly. The data of Fig. 6 are taken from an earlier series of experiments.) A different positioning of the LDA relative to the flow was realized during the collection of these experimental data. In this case, all three LDA components were involved in collecting the data to reduce some problems connected with the defraction of laser beams when they have to cross the shock front in order to reach the measuring volume (refer to the discussion of Fig. 7).

The seeding particles used to obtain the experimental data were introduced into the flow in the settling chamber of the wind tunnel. The distance over which the particles were accelerated to the upstream velocity ahead of the shock is of the order of 50 cm and thus sufficiently long to secure that all seeding particles have adjusted to this flow velocity before reaching the first of the measuring locations of the LDA.

The data points shown in Figs. 6(a) and 6(b) which are interpolated by curves of best fit for better readability of the figure, were obtained for the olive oil seeding particles with the size distribution of Fig. 2. This size distribution was not obtained *in situ*. Nevertheless, additional data of the particle size analysis, other than those presented here in Fig. 2, have shown that the generated particle size distribution of the olive oil seeding particles varies only slightly with the pressure difference between the input and the output side of the Laskin nozzle particle generator used (see Thomas⁹). The particles were led into the settling chamber of the wind tunnel through a tube connected to the particle generator. For the experimental pressure conditions encountered between the settling chamber and the particle generator it can be assumed that the distribution of Fig. 2 represents the size distribution of the olive oil seeding particles effectively fed into the flow.

The adjustments of the LDA system were identical for all runs of the experiment of Fig. 6 except that the amplitude limit and the signal amplification settings were varied from one run of the experiment to the next. The intention of this procedure is to exclude the signals of larger particles from the data evaluation and thus experimentally generate

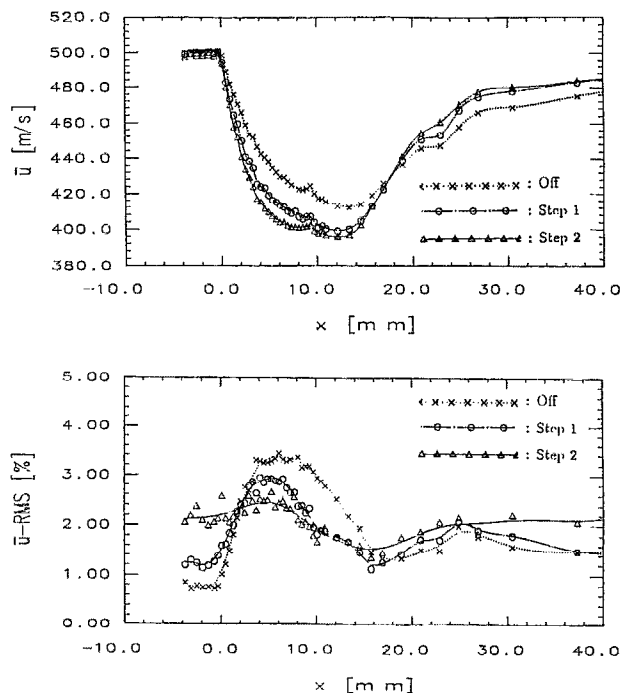


FIG. 6. Experimental results for olive oil seeding particles for the flow velocity across the shock and the pertaining rms value for different settings of the amplitude limit for the flow component in the main flow direction as a function of the coordinate x of the LDA's measuring system.

the situation underlying the numerical results of Fig. 5. This constitutes a realistic approach for the collection of the experimental data presented. By operating the LDA in off-axis mode the length of the effective measuring volume is considerably reduced and the amplitude of the detected signals is almost independent of the exact location of the path taken by the seeding particles within the measuring volume while crossing it. For the curves referred to as "Off" in Figs. 6(a) and 6(b) all detected LDA signals were admitted for data evaluation so long as they only matched the internal requirements of the data acquisition system as to the signal quality. The curve referred to as "Step 1" was obtained after increasing the counters' detected data rate by a factor of approximately five by amplifying the detected signal and then reducing the data rate again to its original value by means of the amplitude limit setting, hence effectively excluding signals with a larger amplitude from data evaluation. The curve referred to as "Step 2" was obtained after repeating the described procedure once more, this time starting from the Step 1 setting. There is an increase of approximately 1% of the rms value upstream of the shock between the data of the Off and the Step 2 runs. This increase has to be attributed to the increased signal amplification, i.e., to the fact that from the original setting Off to the setting Step 1 and finally to the setting Step 2 increasingly weaker and noisier signals are being admitted to the data evaluation. Nevertheless, this does not affect the validity of the qualitative results obtained here.

As can be seen from Fig. 6(a) the continued use of the amplitude limit leads to an increasing slope of the velocity

curves, as is to be expected from the numerical results of Fig. 5(a) discussed above. The increase of the rms value from its value of approximately 0.7% upstream of the shock to the value of around 3.4% at the position of the maximum for the curve referred to as Off lies well within the range to be expected from the curves of Fig. 3(b). The position of the maximum itself is in very good agreement with the position of the maximum of the curve with $\Delta d_p = 1.0 \mu\text{m}$ of Fig. 3(b). The experimental data for the rms value of Fig. 6(b) also show that the overall increase of the rms value from its value just upstream of the shock to its value at the position of the maximum decreases and the width of the interpolation graph through the data points gets narrower while the position of the maximum itself moves towards the shock, as it was also found for the numerical results concerning the usage of the amplitude limit of Fig. 5(b). The overall features of the experimental data observed in Figs. 6(a) and 6(b) thus reveal a very good qualitative agreement with the results of the numerical simulations displayed in Figs. 3 and 5. The fact that the measured curves for the experiment with the amplitude limit switched off compare better to the $\Delta d_p = 1.0 \mu\text{m}$ case than to the $\Delta d_p = 0.0 \mu\text{m}$ case, as would be expected, is most likely to be attributed to a deformation of the olive oil particles during their deceleration after crossing the shock front, as is indicated by the results of another study (see Thomas *et al.*¹⁷). The reacceleration of the flow velocity for $x \gtrsim 13 \text{ mm}$ in Fig. 6 is due to the particles entering the Prandtl-Meyer expansion fan (compare Fig. 1) and being deflected back into the direction of the main flow direction. This reacceleration was neglected in all the numerical calculations discussed above.

Finally, Figs. 7(a) and 7(b) shows some experimental results obtained for different types of seeding particles under very similar flow conditions as before. These results show how the above numerical results can be used to arrive at some qualitative conclusions about the size distributions of seeding particles when their exact size distributions are not known and cannot be measured *in situ*, as is very often the case.

The various seeding materials used were tobacco smoke, incense, and commercially available titanium dioxide (TiO_2) and Blanc Fixe (obtained from PALAS, Karlsruhe, Germany) particles. The average particle diameter \bar{d}_p and the particle density ρ_p of TiO_2 and Blanc Fixe as given by the manufacturer are $\bar{d}_p = 0.35 \mu\text{m}$ and $\rho_p = 4.0 \cdot 10^3 \text{ kg/m}^3$ for the TiO_2 particles and $\bar{d}_p = 0.7 \mu\text{m}$ and $\rho_p = 4.4 \cdot 10^3 \text{ kg/m}^3$ for the Blanc Fixe particles; no information was available about their size distributions. Also shown are data obtained for the olive oil seeding particles used above which are in the remainder referred to as olive oil (cold). The data referred to as olive oil (hot) were obtained with the same olive oil as before but with the oil now having been evaporated and then condensed again before being introduced into the flow as seeding particles (refer to Thomas⁹ for a more detailed description of the process). The particle size analyzer was not available anymore during the course of these experiments so that the only known particle size distribution is that of Fig. 2 for

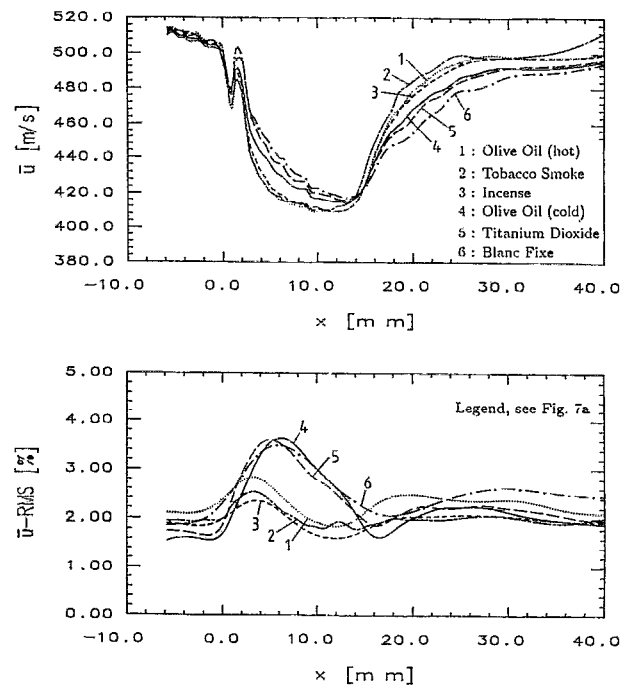


FIG. 7. Experimental results for different types of seeding particles for the flow velocity across the shock and the pertaining rms value for the flow component in the main flow direction as a function of the coordinate x of the LDA's measuring system.

the reference particles, the olive oil (cold) seeding particles.

The experiments employing the different types of seeding materials were carried out without the amplitude limit being effective. In order to keep the adjustments of the LDA system as identical as possible for all runs while still obtaining sufficiently high data rates for all the different types of seeding materials used, a setting of the system had to be accepted which led to a relatively high rms value of around 1.4% just upstream of the shock for the olive oil (cold) reference particles. Nevertheless, a slightly increased signal amplification rate for the incense, tobacco smoke, and the olive oil (hot) seeding particles had to be allowed for.

For the sake of clarity the actual data points of the results were omitted in Fig. 7 and only smoothed curves obtained by spline interpolations are shown. The distance between two successive measuring locations of the results of Fig. 7 was, as in Fig. 6, approximately 0.4 mm for any location $x \lesssim 12 \text{ mm}$ and of the order of 1-2 mm for measuring locations $x \gtrsim 12 \text{ mm}$. The apparently rather large velocity fluctuation in the region $0 \lesssim x \lesssim 2 \text{ mm}$ is spurious; it does not reflect a real change of the flow velocity. This fluctuation is due to the orientation of the LDA's laser beams relative to the main flow direction, i.e., relative to the shock inside the wind tunnel's test section. For the results of this particular set of experiments shown in Figs. 7(a) and 7(b) the orientation of the LDA relative to the shock was such that for the interval $0 \lesssim x \lesssim 2.0 \text{ mm}$ of measuring locations one beam at a time of the LDA's beam pair involved in collecting the velocity data for this velocity

component had to cross the shock front in order to reach the measuring volume. Due to the density change across the shock this beam was deflected out of its original direction. Thus the angle between the two beams of that beam pair was changed, leading to the collection of erroneous velocity data in this region.

Figure 7(a) shows that the best experimental results, i.e., the smallest relaxation length to the downstream flow velocity and the smallest contribution to the rms value, is obtained for the olive oil (hot) and the tobacco smoke seeding particles. Whereas the experimental results for the incense do not vary too much from the olive oil (hot) and the tobacco smoke results, especially the results for the solid TiO_2 and the Blanc Fixe particles and less so the results for the olive oil (cold) particles show a considerably worse relaxation behavior, as can be seen in Fig. 7(a). These larger types of particles also bias the experimental results to a much larger extent than the olive oil (hot), tobacco smoke and incense particles as can be seen from Fig. 7. Figure 7(b) shows that the rms value for the results of the smaller particles [incense, tobacco smoke, olive oil (hot)] takes on its maximum closer to the shock than it does for the larger particles [TiO_2 , Blanc Fixe, olive oil (cold)]. The rms value for the smaller particles increases across the shock by about a maximum of around 0.5% in contrast to around 2% for the bigger particle types, indicating that the smaller particles also have a less broad size distribution.

As the TiO_2 particles probably have a size distribution corresponding to a lower standard deviation than the olive oil (cold) particles it may be surprising that both seeding materials show nearby results for their rms values. To explain this observation it has to be taken into consideration that the density of the TiO_2 is approximately four times greater than the density of the olive oil (cold). The numerical results of Fig. 4(b) indicate that this difference of their densities can account for a considerable spreading of the width of the rms curve and also for a significant downstream shift of the position of the maximum rms value. A decreasing average diameter leads as follows from Fig. 3(b) to an upstream shift of the position of the maximum rms value, to a narrowing of the rms curve and possibly to a growth of the absolute maximum rms value. The effects of a smaller standard deviation can be inferred from Fig. 5(b) which shows that these effects are also an upstream shift of the position of the rms maximum and a narrowing of the width of the rms curve together now with a simultaneous decrease of the maximum rms value. Moreover Figs. 3–5 indicate that the absolute upstream shift of the position of the rms curve's maximum shows a weaker dependence on a decreasing standard deviation and also a weaker dependence on a decreasing average particle size than the absolute downstream shift of this position depends on the particle density for the density range considered here. An interaction of all of these observed effects may well be responsible for the similarity of the obtained experimental rms data for the olive oil (cold) and the TiO_2 seeding particles.

The comparison of the results obtained for the olive oil

(cold) and the olive oil (hot) of Fig. 7 show that the procedure of evaporating and condensing the olive oil before introducing it into the flow as seeding particles has led to a significant improvement of the seeding particles and thus of the experimental results obtained. It can be concluded that the olive oil (hot) seeding particles possess a smaller average particle size and a narrower size distribution than the initial olive oil (cold) particles. This can be regarded as an additional experimental result and it is suggested to employ this simple technique to improve the liquid seeding particles in future experimental studies.

IV. CONCLUSION

It has been shown how the properties of the size distribution of seeding particles influence the results of LDA velocity measurements in the vicinity of a large velocity gradient. The average velocity and the pertaining rms value to be expected in the relaxation region immediately downstream of an aerodynamic shock within which the seeding particles adjust to the changed flow velocity were numerically determined. It was shown how both quantities depend on the size distribution of the seeding particles and on the density of the particle material. It was demonstrated by numerical simulation how the LDA's data evaluation system's amplitude limit, which can offer means of excluding large particles from data evaluation, affects the average velocity and the rms value when increasingly more and more particles on the "large particle side" of the size distribution are neglected. The numerical results were compared to experimental LDA velocity data collected in the downstream region of an oblique aerodynamic shock using different types of seeding particles. A good qualitative agreement between experiment and numerical simulation was found.

The results presented clearly show the importance of the contribution due to the size distribution of the seeding particles towards the total rms value. This contribution in a region of, or right downstream of, a large velocity gradient might easily mask possible real velocity changes in certain applications. It is therefore of great importance, unless nearly monodisperse seeding particles should become readily available for all measuring applications, to carefully consider beforehand the magnitude of this contribution for one's specific measuring configuration. If the small-scale structure of the flow field to be monitored is not already known, and large velocity gradients may be expected, no reliable interpretation of any collected experimental tracer technique velocity data can be given without a prior, careful consideration of the relaxation behavior towards large velocity gradients of the seeding particles fed into the flow.

In conclusion, it is suggested that any future study concerned with a numerical investigation of the influence of the size distribution of seeding particles on the results of LDA velocity measurements should consider an analytic law (for example a law of lognormal form) to define the polydisperse character of different aerosols in order to obtain a greater generality of the results. Nevertheless, extreme care has to be taken in a quantitative comparison

between experimental and numerical results, as it was shown by Thomas *et al.*¹⁷ that the degree of agreement of particle motion calculations and experimental data may depend on the exact flow conditions as well as on the deformability of the particles.

ACKNOWLEDGMENT

The authors would like to thank Dr. H.-G. Horn at TSI, Aachen, Germany for the size analysis of the olive oil seeding particles.

- ¹B. R. Maxwell and R. G. Séasholtz, "Velocity lag of solid particles in oscillating gases and in gases passing through normal shock waves," NASA Tech. Note TN D-7490 (1974).
- ²M. J. Walsh, "Influence of drag coefficient equations on particle motion calculations," Proceedings of the Symposium on Laser Anemometry, University of Minnesota, Bloomington, MN, 22-24 October 1975.
- ³R. H. Nichols, "Calculation of particle dynamics effects on laser velocimeter data," in *Wind Tunnel Seeding Systems for Laser Velocimeters*, NASA Conf. Publ. 2393, Workshop at Langley Research Center, 19-20 March 1985.
- ⁴G. Tedeschi, H. Gouin, and M. Elena, "Etude theoretique du suivi de particules dans les ecoulements a forts gradients de vitesse," Actes du 2ème Congres Francophone de Velocimetrie Laser, Meudon, France, 25-27 September 1990.
- ⁵M. S. Maurice, "Laser velocimetry seed particles within compressible, vortical flow," *AIAA J.* **30**, 376 (1992).
- ⁶V. Krishnan, K.-A. Bütefisch, and K. H. Sauerland, "Velocity and turbulence measurements in the shock region using the two component laser Doppler anemometer," *Proceedings of the ICALEO 1987, Optical Methods in Flow and Particle Diagnostics*, edited by W. H. Stevenson (The Laser Institute of America, Toledo, OH, 1987), Vol. 63.
- ⁷C. d'Humieres, F. Micheli, and O. Papirnyk, "Etude du Comportement des Aerosols pour la Mesure en Velocimetrie Laser," Actes du 2ème Congres Francophone de Velocimetrie Laser, Meudon, France, 25-27 September 1990.
- ⁸S. L. Soo, *Fluid Dynamics of Multiphase Systems* (Blaisdell, Waltham, MA, 1967).
- ⁹P. Thomas, "Experimentelle und theoretische Untersuchungen zum Folgeverhalten von Teilchen unter dem Einfluss grosser Geschwindigkeitsgradienten in kompressibler Strömung," Doctoral Thesis, University of Göttingen [published by Deutsche Forschungsanstalt für Luft- und Raumfahrt as Research Report DLR-FB 91-25 (1991)].
- ¹⁰R. R. Hughes and E. R. Gilliland, "The mechanics of drops," *Chem. Eng. Prog.* **48**, 497 (1952).
- ¹¹P. J. Thomas, "On the influence of the Basset history force on the motion of a particle through a fluid," *Phys. Fluids A* **4** (1992).
- ¹²C. B. Henderson, "Drag coefficients of spheres in continuum and rarefied flows," *AIAA J.* **14**, 707 (1976).
- ¹³H. W. Press, B. P. Flannery, S. A. Teukolsky, and W. T. Vetterling, *Numerical Recipes, The Art of Scientific Computing* (Cambridge University Press, Cambridge, 1986).
- ¹⁴W. H. Echols and J. A. Young, "Studies of portable air-operated aerosol generators," NRL Report 5929, U.S. Naval Research Laboratory, Washington, D.C., 1963.
- ¹⁵K.-A. Bütefisch and K. H. Sauerland, "A three component dual beam laser-Doppler-anemometer to be operated in large wind tunnels," Proceedings of the ICIASF '85, Stanford University, 26-28 August 1985.
- ¹⁶K.-A. Bütefisch, "Three component laser Doppler anemometry in large wind tunnels," *Prog. Aerosp. Sci.* **26**, 79 (1989).
- ¹⁷P. J. Thomas, K. A. Bütefisch, and K. H. Sauerland, "On the motion of particles in a fluid under the influence of a large velocity gradient," *Exp. Fluids* **14**, 42 (1993).